Journal of The Electrochemical Society, **152** (8) A1526-A1532 (2005)
0013-4651/2005/152(8)/A1526/7/$7.00 © The Electrochemical Society, Inc.

Enhanced High-Rate Cycling Stability of $LiMn_2O_4$ Cathode by ZrO_2 Coating for Li-Ion Battery

Yong-Mao Lin,[a] Hung-Chun Wu,[b] Yu-Chan Yen,[a] Zheng-Zhao Guo,[b] Mo-Hua Yang,[b] Hui-Min Chen,[c] Hwo-Shuen Sheu,[d] and Nae-Lih Wu[a,*,z]

[a]*Department of Chemical Engineering, National Taiwan University, Taipei, Taiwan 106*
[b]*Materials Research Laboratories, Industrial Technology Research Institute, Chutung, Hsin-Chu, Taiwan 310*
[c]*Taipei Medical University, Taipei, Taiwan 110*
[d]*National Synchrotron Radiation Research Center, Hsinchu 30077, Taiwan*

The effect of a sol-gel derived amorphous zirconium oxide surface coating on the high charge-discharge (CD) rate performance of $LiMn_2O_4$ was studied. When cycled between 4.5 and 2.9 V (vs. Li/Li^+) at room temperature, the coated spinel electrode, containing 5 wt %-ZrO_2, shows tremendous enhancement in cycling stability at CD rates up to 10 C. Concurrently, the coated spinel electrode exhibits a lower cubic-tetragonal transition potential, a smaller charge-transfer impedance by 4-5-fold, and it profoundly reduces, by 66%, lattice contraction upon charge (delithiation). The enhancement in the high-rate cycling stability has been attributed to the combination of these favorable effects.
 [DOI: 10.1149/1.1945727]

Manuscript submitted November 24, 2004; revised manuscript received January 30, 2005. Available electronically June 28, 2005.

Cubic spinel $LiMn_2O_4$ is of great interest for the replacement of $LiCoO_2$ in Li-ion batteries due to its high voltage, natural abundance, low cost, and environmental benignity.[1-3] Particular enthusiasm has been shown to use this material in electric vehicle application owing to its superior safety properties to $LiCoO_2$.[4,5] For this application, however, high-rate cycling stability will be one major issue. The discharge (lithiation) potential signatures in $Li_xMn_2O_4 (x \leqslant 1)$ include two large plateaus near 4.1 and 4.0 V (all the potentials referred to herein are referenced to Li/Li^+),[6] which have been suggested[7] to involve transitions among three cubic phases. Insertion of Li for $x > 1$ results in another plateau near 2.8 V, corresponding to the transition from cubic $LiMn_2O_4$ to tetragonal $Li_2Mn_2O_4$. The phase transition involves Jahn-Teller distortions, associated with Mn^{3+} Jahn-Teller ions.[8]

The spinel exhibits faster capacity fading upon charge-discharge (CD) cycling than $LiCoO_2$, and the cubic-tetragonal (CT) transition, which involves a large (~10%) unit cell volume variation, has been considered as one important cause to the fading at room temperature (RT).[9] When a $LiMn_2O_4$ electrode is discharged in the practical full-cell operation, the Li concentration gradient is expected to develop throughout the particle, and the Li stoichiometry, x in $Li_xMn_2O_4$, at particle surface may be well above 1.0, even when the average stoichiometry is less than 1.0. This was evidenced by microscopy analysis, which showed the presence of the tetragonal surface layer.[10] The higher the discharge rate is, the more pronounced this surface transition effect is expected to be. Accordingly, the fading rate of the spinel is expected to increase appreciably with CD rate. Capacity fading of the spinel is also increasingly serious with increasing temperature, and it has in part been attributed to the degradation of the spinel by dissolution of Mn ions into the acidic electrolyte.[11,12]

Some studies (e.g., Ref. 13 and 14) showed the substitution of Mn at the 16d sites with ions with a valence $\leqslant +3$ to give doped spinels $Li_xM_yMn_{2-y}O_4$ (M = Ti, Fe, Ni, Co, Zn, Al, and Mg), which could enhance the cycling stability at RT. Although this approach has improved the structural stability, it seriously reduces initial capacity. As an example, our test on a commercially available Al-doped spinel having the nominal composition of $Li_{1.10}Al_{0.095}Mn_{1.805}O_4$ showed an initial capacity at 0.2 C rate of merely 108 mAh/g for the 4 V plateaus, in contrast with >120 mAh/g typically for the nondoped spinel (see later).

Surface coating with transition metal oxides has been shown as an effective way to improve cycling stability for some cathode materials of Li-ion battery. For $LiMn_2O_4$, Thackeray et al.[15] have indeed shown that the high-temperature cycling stability of the spinel is significantly improved by surface coating of amorphous Zr oxide. The improvement has been attributed to the reduced solubility of the spinel as a result of scavenge of acidic HF in the electrolyte by the Zr oxide layer. The effect of the coating on the RT cycling stability has, however, not been elucidated. Indeed, as the oxide coating is an electronic insulator, there is concern over its effect on high-rate performance of the spinel electrode.

As reported in this work, coating the spinel $LiMn_2O_4$ with an amorphous Zr oxide layer resulted in a tremendous improvement in cycling stability at RT at as high a rate as 10 C. This is the first time that an oxide coating has been reported to exhibit enhancement in cycling stability under such a high CD rate. Studies based on impedance and in situ synchrotron X-ray diffraction (XRD) analyses also indicated that the coated spinel exhibited remarkably different reaction impedance and lattice variation characteristics from the uncoated one during CD cycling.

Experimental

$LiMn_2O_4$ was used as received from Sedema (Tertre, Belgium). For making the Zr oxide coating layer, Zr butoxide [~80% $Zr(OC_4H_9)_4$ in *tert*-butanol, Aldrich] was mixed with 1-butanol in a volume ratio of alkoxide/alcohol = 1:4 under ultrasonic agitation for 30 min. Selected amount of $LiMn_2O_4$ powder was then dispersed into the coating solution, followed by settling under vacuum. The air trapped inside the spinel powder was drawn out at low pressure, and this step was meant to facilitate good contact between the coating solution and the powder. The dispersion solution was then heated to 75°C for 8 h with continuous stirring and slowly introducing water vapor into the solution. Slow hydrolysis and drying is the key to the formation of conformal coating. Finally, the coated powder was calcined at 400°C, ground, and sieved.

The spinel electrode was made of 88 wt % $LiMn_2O_4$ powders, either with or without the Zr oxide coating, 6 wt % carbon black, and 6 wt % poly-(vinylidene fluoride) (PVdF) on an Al current collector. After being dried at 150°C in a vacuum oven for 24 h, the electrode sheets were punched into 1.2 cm diameter disks for assembly; every disk typically contains ~9 mg of the spinel with 70 μm thickness. The coin cell consists of a spinel disk electrode, a Li foil disk as the counter electrode, and electrolyte of 1 M $LiPF_6$ in a 50/50 (vol %) mixture of ethylene carbonate (EC) and ethyl methyl carbonate (EMC). All the cells were assembled in a dry room where the dew point was maintained at between −40 and −45°C.

CD cycles were recorded using a galvanostatic cycling system

* Electrochemical Society Active Member.
z E-mail: nlw001@ntu.edu.tw

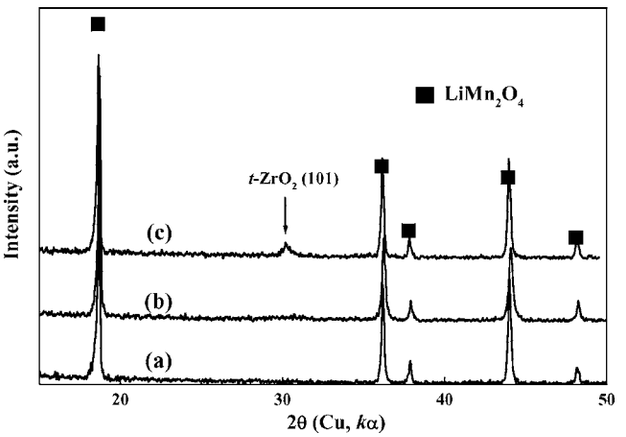

Figure 1. XRD (Cu Kα) patterns of $LiMn_2O_4$ powders: (a) no coating; (b) coating with 5% ZrO_2 and calcined at 400°C; and (c) calcined at 600°C.

(BT-204, Arbin Corp.). The CD rate is calculated on the basis of the theoretical capacity (148 mAh/g of the spinel. Accordingly, 1 C rate corresponds to a current density of ~1.2 mA/cm^2 in the present setup. An AUTOLAB frequency response analyzer (AUTOLAB, Eco Chenie PGSTAT30) was employed for obtaining complex impedance spectra in the frequency range from 1 mHz to 10 kHz.

Powder X-ray diffraction (XRD) analysis was performed with a Philips diffractometer, using Cu Kα radiation and a graphite monochromator. Synchrotron XRD was carried out by using beam-line 01-C2 facilities of the National Synchrotron Radiation Research Center in Taiwan. The wavelength of the X-ray is 0.061 993 nm. In situ XRD patterns were acquired during the course of a CD cycle at 0.5 C rate. The corresponding potential curve was simultaneously recorded. The covers of both sides of the cell were first perforated and then sealed with Kapton foils in order to allow the X-ray beam to pass through the cell. Diffraction patterns were recorded by a curved translating imaging plate (Fuji BAS2500) with the sample-to-film distance of 280 mm. Two-dimensional diffraction data were converted to one-dimensional profile using the FIT2D program.[16] Particle morphology was analyzed by a scanning electron microscope (SEM; Hitachi, S-800), and the cross-sectional images were taken by using a transmission electron microscope (TEM; Hitachi H-7100). To prepare the TEM specimen, the oxide powders were embedded in a epoxy resin made of alraldite-520 resin, EPON-812, dodecenyl succinic anhydride, and 2,4,6-tri(dimethylaminomethyl) phenol (hardener) with 6:18:10:1 in volume ratio, and sliced with an ultramicrotome.

Results

Because of the nature of the coating process, all the Zr in the coating solution was eventually deposited onto the surfaces of the spinel particles. Powders having different coating loadings were obtained by predetermining the amounts of Zr butoxide in the coating solution. Although the coating was amorphous in nature (shown below), for brevity, the coating loading is hereafter expressed in terms of the weight fraction in ZrO_2 stoichiometry, and the spinel powders and the electrodes made of the powders are referred to by their ZrO_2 loadings. (Accordingly, the 0% electrode is for the electrode consisting of uncoated spinel powder.) Powders having four different coating loadings, including 0 (bare), 1, 3, 5, and 7 wt %, were prepared and tested, but mainly the results acquired from the 0 and 5% powders are presented in this paper, as they were most thoroughly studied. Nevertheless, it is worth mentioning that the results from the other two powders follow the same trends.

Powder XRD study (Fig. 1) showed that, for either the bare or coated powders calcined at 400°C, only the reflections of $LiMn_2O_4$ were observed. When the calcination temperature was raised to 600°C (curve c), reflections of tetragonal ZrO_2 began to be detected. These results indicate that the Zr oxide coating on the powders calcined at 400°C exists mainly as an amorphous phase, and it does not crystallize until 600°C.

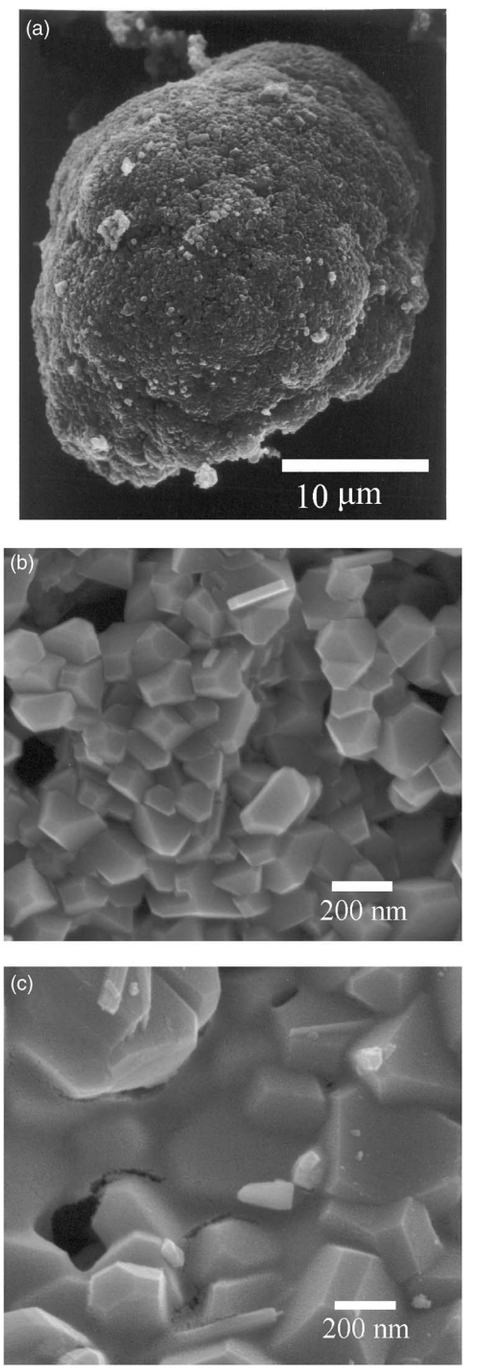

Figure 2. SEM micrographs of $LiMn_2O_4$ powders with different Zr oxide coating contents: (a), (b) no coating; (c) 5% ZrO_2.

SEM analysis showed that the as-received $LiMn_2O_4$ particles have a rounded morphology and sizes in the range of 15-30 μm (Fig. 2a), and each particle is composed of many primary faceted crystallites with a size of ~0.2 μm (Fig. 2b). For the coated powders (Fig. 2c), many crystallites exhibited similar morphology to the uncoated ones. However, by following the micrographs of powders of increasing ZrO_2 content ranging from 1 to 7%, we can see the

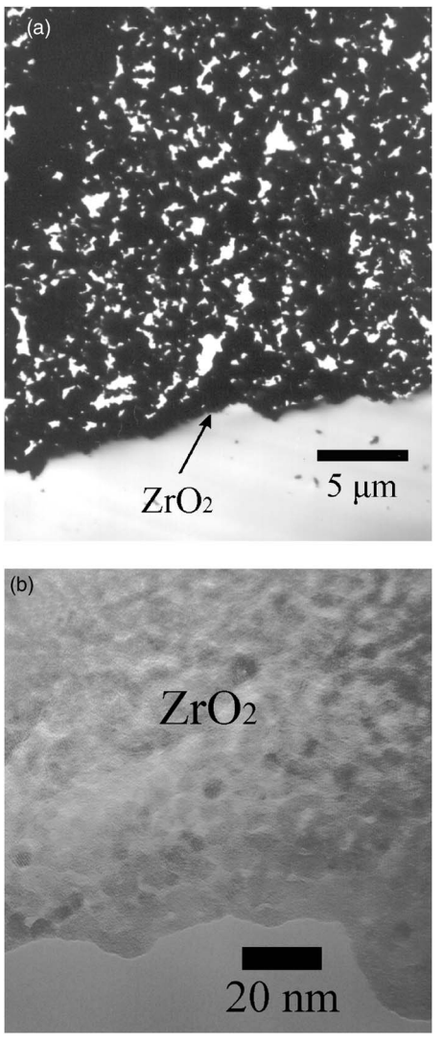

Figure 3. Cross-sectional TEM micrographs of the ZrO_2-coated $LiMn_2O_4$ powder: (a) the particle; (b) the coating layer.

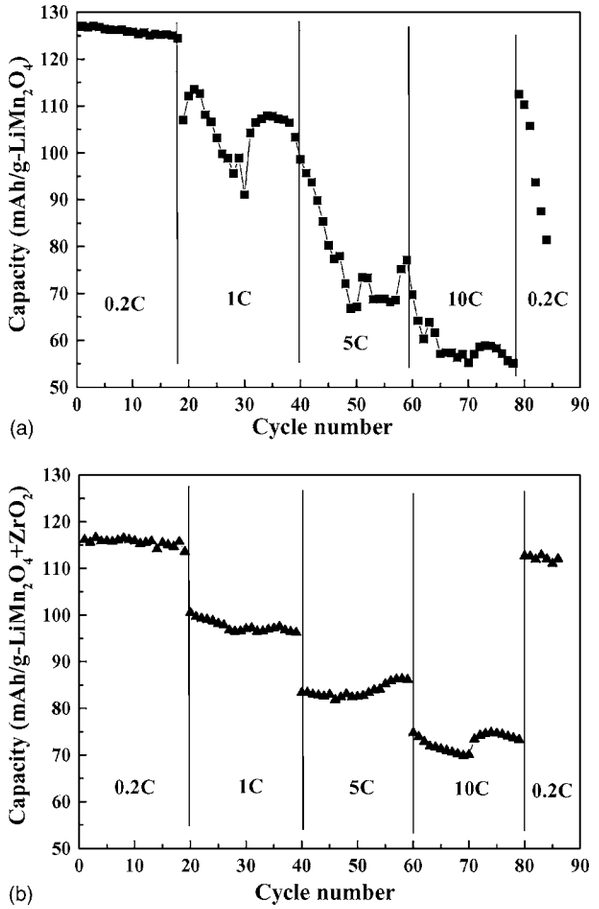

Figure 4. The discharge capacity vs. cycle number under different CD rates at room temperature: (a) the bare-$LiMn_2O_4$ electrode; (b) the 5% ZrO_2 electrode. The CD rates are expressed in C-rate.

edges of the faceted crystallites become increasingly rounded, indicating the presence of conformal coating layer with increasing thickness. No individual Zr oxide particles have been observed. As mentioned earlier, slow hydrolysis and drying is the key to the formation of conformal, uniform coating. Distinct thick coating layers typically occur either in the valleys between adjacent crystallites or covering pores. TEM analysis showed that the interior of the particles remain porous even after the coating process (Fig. 3a). High-resolution TEM indicated that the coating layer is nonporous and amorphous in nature (Fig. 3b).

The CD cycling tests have been performed at consecutively increasing C rates, from 0.2 to 10 C, with 20 cycles at each selected C rate. Figure 4a and b summarizes the discharge capacity data throughout the tests for the 0 and 5% electrodes, respectively. Figure 5a and b shows the potential curves for selected cycles. For the 0% electrode, it has an initial capacity of 127 mAh/g-$LiMn_2O_4$, and exhibits a capacity fading rate of 0.15 mAh/g cycle at 0.2 C. Upon step increases in the CD rate, the capacity was found to descend rapidly in unstable patterns to lower levels. At $\geqslant$5 C, the capacity and Coulombic efficiency continuously decrease with increase in both CD rate and cycle number. When the CD rate was reduced back to 0.2 C, the capacity first returned to almost the initial capacity once but subsequently faded very rapidly (fading rate: 6.0 mAh/g cycle) (Fig. 4a).

Two major discharge plateaus at ~4.1 and 4.0 V, respectively, are clearly shown at 0.2 C. When the CD rate was increased to 1 C, the entire potential curve shifted to a lower potential level by ~0.1 V, and it is believed to be largely due to IR drop. With further increasing CD rate, the entire curve became increasingly inclined, while the two plateaus remain distinct from each other with the lower-potential plateau bent faster than the higher-potential plateau.

Coating with the Zr oxide layer was found to result in the following effects on the CD behaviors. First, the initial capacity is slightly reduced. The initial capacity of the 5% ZrO_2 electrode is 116 mAh per gram of the active material ($LiMn_2O_4$ + ZrO_2), which corresponds to 122 mAh per gram of $LiMn_2O_4$, if the entire discharge capacity is attributed to the spinel. Second, upon a step increase in CD rate, the capacity showed an immediate descent to a lower capacity level, at which the capacity basically remains quite stable within 20 cycles (Fig. 4b). There appears some instability at 10 C, probably because the current is approaching the limit of the coin-cell test. In any case, it is still much more stable than the 0% electrode. Third, the capacity regained 97% of the initial capacity when the CD rate was subsequently reduced back to 0.2 C and remained stable. The Coulombic efficiency remained better than 98% for all cycles. Finally, at CD rate $\geqslant$1 C, the potential curve was found no longer to exhibit two plateaus but one inclined plateau (Fig. 5b).

In a separate test with an expanded CD potential range, it was found that discharging the electrodes to a lower potential range caused the occurrence of an additional plateau near 2.8 V, associated with the CT transition for all the electrodes. However, the CT

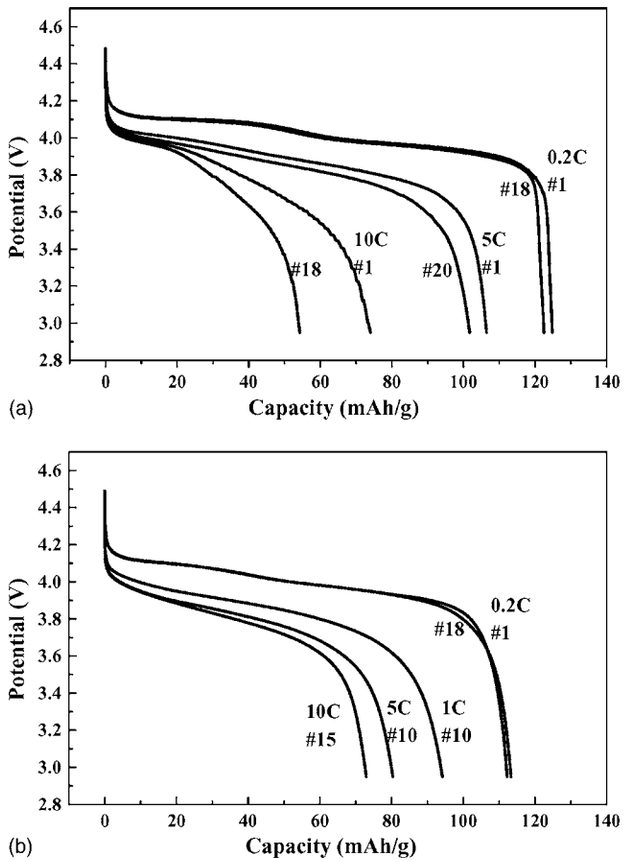

Figure 5. The potential curves for cycling under different rates: (a) the bare $LiMn_2O_4$ electrode; (b) the 5% ZrO_2 electrode.

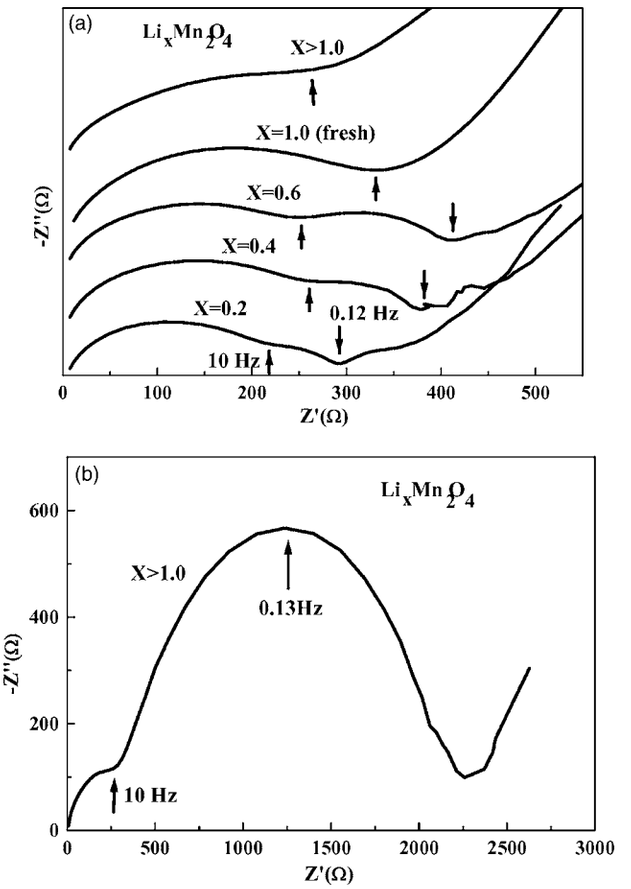

Figure 7. Nyquist plots for the bare $LiMn_2O_4$ electrode during the discharge (lithiation) stage. (a) Plots at different discharged states. The plots have been shifted along the *y* axis for clarity. (b) The plot for $x > 1.0$ (discharged to 2.8 V) with a larger *x*-axis scale than in (a). The up- and down arrows locate the data points of 10 and 0.12 Hz, respectively.

plateau of the 5% electrode occurred at a potential (2.79 V) slightly lower than that (2.87 V) of the 0% ZrO_2 electrode (Fig. 6). The potential difference in general increases with increasing amount of coating from 3 to7 wt % ZrO_2.

Alternating current (ac) impedance analysis was carried out by first taking a spectrum at the fresh state, then fully charging the cell to 4.5 V and finally acquiring spectra at selected depth of discharge (lithiation). For the 0% electrode with the Li stoichiometry $x \leqslant 1.0$ (Fig. 7a), there are two semicircles at frequencies $\geqslant 0.12$ Hz. The high-frequency ($\geqslant 10$ Hz) semicircle can be attributed to the impedance of surface film, while the intermediate-frequency semicircle, between 10 and 0.12 Hz, can be attributed to the charge-transfer impedance. The inclined line below 0.12 Hz is associated with bulk diffusion of Li^{+2}. The nonlinearity of this inclination line observed for $x < 0.6$ may result from significant heterogeneity in composition within the interior of the spinel particles during the early stage of the lithiation process. Both the thin film and charge-transfer resistances were found to increase with increasing depth of lithiation. The curves were approximately the same between the fresh electrode and the one that was subjected to one cycle back to $x = 1.0$. Finally, an extremely large resistance ($\sim 2000\ \Omega$) occurred when the electrode was lithiated to $x > 1.0$ (Fig. 7b).

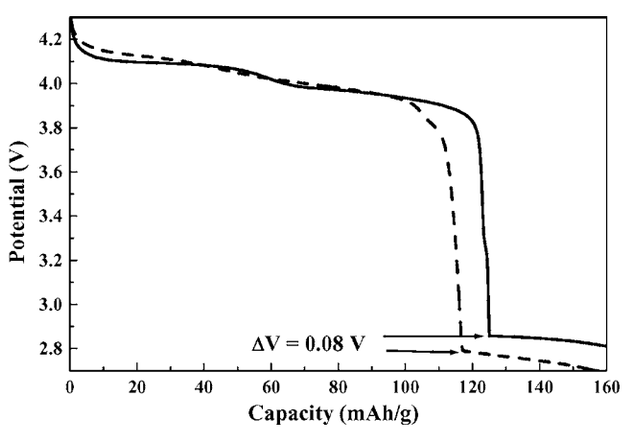

Figure 6. The potential curves showing the potential difference of the CT plateau: (solid line) the bare $LiMn_2O_4$ electrode; (dashed line) the 5% ZrO_2 electrode.

The Nyquist plots of the 5% electrode showed similar line profiles (Fig. 8a) to the 0% electrode, exhibiting two semicircles followed by a low-frequency inclination line. In this case, the first circle should be assigned to the impedance from the combination of the coating and surface thin film. Overall, the coated-spinel electrode exhibited much smaller, by 4-5-fold reduction, thin-film and charge-transfer resistances. It was further noticed that when an electrode completed one cycle back to $x \sim 1.0$, the resistances became much smaller than those of the fresh electrode (Fig. 8b). The results indicate that the interface resistance is reduced by the Zr oxide coating only after the coating has been lithiated.

By using in situ synchrotron XRD study of $LiMn_2O_4$ electrode,

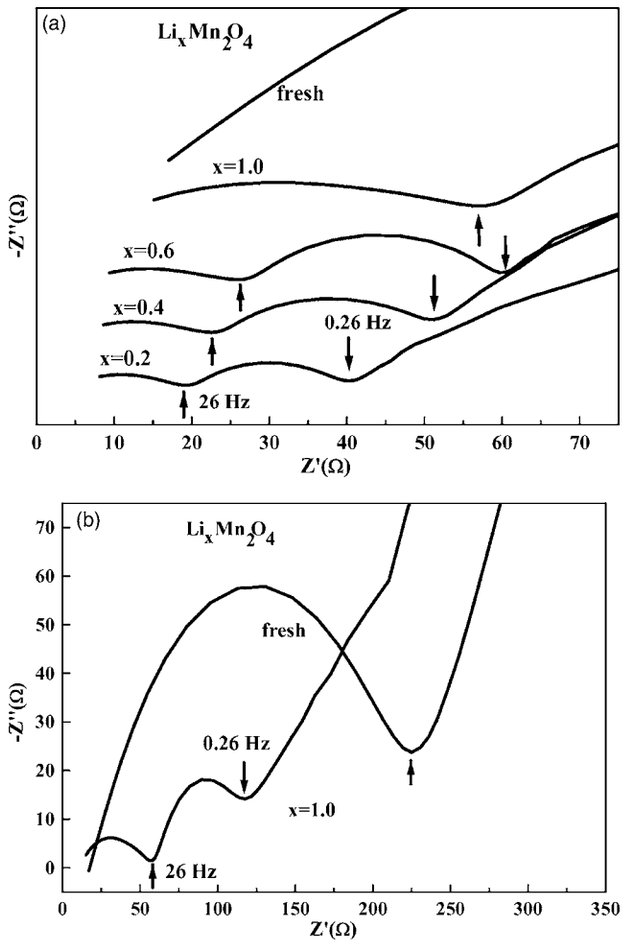

Figure 8. Nyquist plots for the 5% ZrO_2 electrode during the discharge (lithiation) stage. (a) Plots at different discharged states. The plots have been shifted along the *y* axis for clarity. (b) Comparison between the fresh electrode and the one complete cycle ($x = 1.0$). The up- and down arrows locate the data points of 26 and 0.26 Hz, respectively.

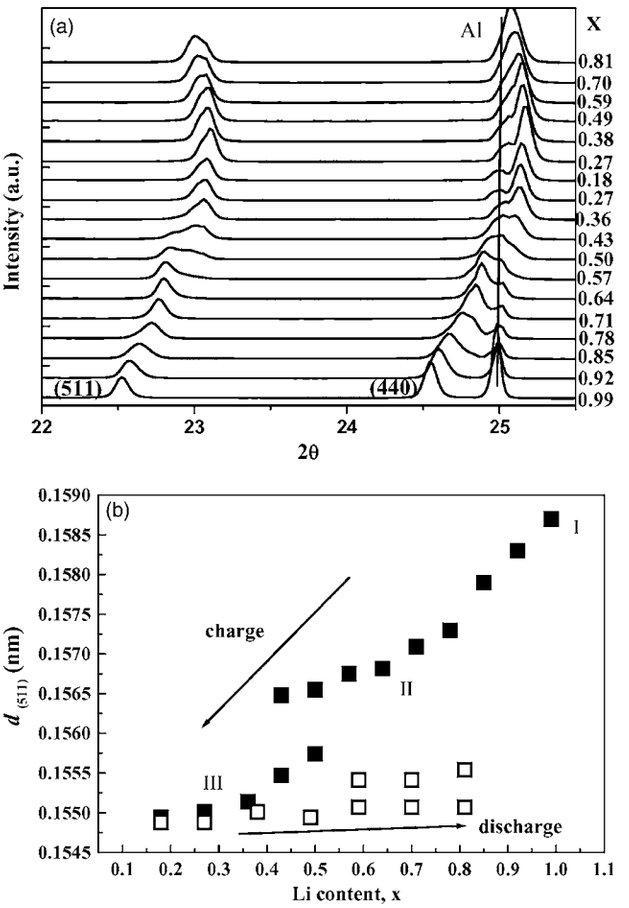

Figure 9. In situ synchrotron XRD data for the bare $LiMn_2O_4$ electrode during the course of a charge-discharge cycle: (a) the XRD patterns; (b) the (511) *d*-spacing data vs. Li stoichiometry *x* in $Li_xMn_2O_4$.

Sun et al.[7] previously suggested that the two-stage 4 V plateaus involve structural transition between three cubic phases. The transition characteristics appearing in their XRD data were also observed during the first charge phase of our 0% electrode. Figure 9a showed the synchrotron XRD patterns acquired during the course of a CD cycle of the 0% electrode, while Fig. 9b summarizes the change in lattice spacing of a selected reflection (511) of the spinel. The notations for the three cubic phases, cubic I, II and III, used by Sun et al., is adopted here. The Li stoichiometry (x) was determined from the potential curve that was simultaneously recorded. As indicated in Fig. 9b, the cubic I and II phases can be differentiated by their different rates in lattice contraction, while the transition between cubic II and III are indicated by a sudden jump in lattice spacing within the range of $x = 0.55$-0.35. Overall, the lattice spacing of the (511) reflection shrank by 2.4% during charge from $x \sim 1.0$ to 0.18.

The structure of the spinel was not restored upon discharge but showed significant irreversibility in lattice structure (Fig. 9a and b), despite the fact that the potential curve indicated ~85% restoration in capacity. (Control study indicated that the loss is due to humidity leakage through the holes drilled on the covers of the cell for the passage of the X-ray beam.) Transition from cubic III to cubic II was never completed. Structural irreversibility was barely seen in Sun's work,[7] which employed a discharge rate about one third of that in the present work. These results may indicate that the structural transitions upon lithiation encounter greater energy barriers and hence proceed with slower rates than those in delithiation. The former involve unit-cell expansion, and the latter unit-cell contraction.

For the 5% electrode, synchrotron XRD data indicated much milder variation in lattice structure upon charge (Fig. 10a and b). The lattice spacing of the (511) reflection, for instance, shrank by only 0.76% upon charge from $x \sim 1.0$ to 0.18, in contrast to 2.4% for the 0% electrode (Fig. 9b). Notably, the (511) *d*-spacing appearing at the end of the first charge ($x \sim 0.18$) phase of the 5% electrode is even larger than that of the 0% electrode after the discharge phase ($x \sim 1.0$) (Fig. 9b and 10b). Furthermore, the 5% electrode no longer showed the sudden jump in lattice spacing from cubic II to III, even though the charge potential curve did show the two-stage plateau characteristics basically the same as those of the 0% electrode.

Linewidth analysis on the (511) peak shows that the full width at half-maximum intensity increases monotonically with decreasing x up to the maximum of ~20%, broadening upon charge to $x = 0.14$. The monotonic behavior of the XRD line broadening indicates that it is single-phase behavior but not due to overlapping of the lattice parameters of multiple phases. The broadening may be due to decrease in crystal size or strain built up within the crystal lattice.

The lattice parameter remained unchanged (Fig. 10b) upon discharge, while the linewidth decreases toward the original width upon discharge. The lattice structure is expected to remain unchanged during the subsequent cycles because the spacing is already

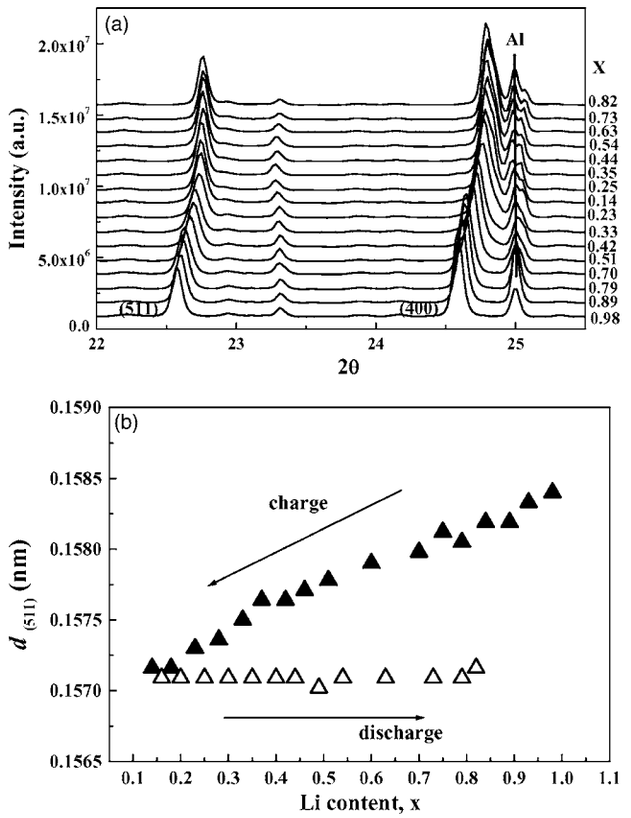

Figure 10. In situ synchrotron XRD data for the 5% ZrO_2 electrode during the course of a charge-discharge cycle: (a) the XRD patterns; (b) the (511) *d*-spacing data vs. Li stoichiometry x in $Li_xMn_2O_4$.

the smallest limit during the first charge phase and no contraction would take place upon the second and subsequent cycles.

Discussion

The CD cycling data shown above clearly demonstrate that coating with Zr oxide can significantly enhance the cycling stability of $LiMn_2O_4$ under high-rate conditions at RT. Concurrently, several original effects which might contribute to the enhancement have been detected, including (*i*) delay in CT transition toward lower potentials; (*ii*) reduction in reaction impedance; and (*iii*) reduced structural variations involved during the lithiatin/delithiation reactions.

This "delaying" effect was initially thought to arise from a larger polarization due to the presence of an insulating ZrO_2 coating. However, the impedance results quickly disapproved the reasoning because the electrode constituted of the coated powder actually exhibits a lower overall resistance to the lithiation/delithiation processes. That is, the introduction with such a small amount of electronically insulating coating does not impose significant resistance to the entire electrochemical process. This result may also suggest that the rate-limiting step for the process does not lie in the charge transfer between particles but primarily at the solid/electrolyte interface.

ZrO_2 can form several thermodynamically stable phases with Li,[17] suggesting possible high solubility of Li in an amorphous ZrO_2 matrix. In this case, the Zr oxide coating could serve as a highly Li-conducting SEI (solid electrolyte interface)[15] that provides an additional reaction pathway of lower resistance. This is consistent with the results showing that the reduced resistance occurs only after the first charge step, i.e., when the coating is lithiated. The presence of a fast Li-ion conductor along with a reduction in the interfacial reaction resistance can help to reduce Li concentration gradient throughout the electrode and thereby minimize the chance of accumulation of excess Li ions to the level of $x > 1.0$ at certain sites, which would otherwise go through the CT transition "earlier," i.e., at higher potentials. This may be one cause of the "delayed" occurrence of the CT transition by the Zr oxide coating, and accordingly it can contribute to the enhancement in cycling stability of the spinel, particularly under high-rate conditions.

The mechanism via which the CT transition affects the capacity fading has not been unequivocally established. Some suggest that it has to do with the large (10%) unit-cell volume expansion from cubic I to the tetragonal phase. Indeed, the synchrotron XRD data shown in this work give strong indication that lattice expansion with such a magnitude would never be completed under high-rate conditions. Thus, one possible cause of the capacity fading is that structure defects are created when excess Li ions ($x > 1.0$) are forced electrochemically to go into the cubic lattice while the structure fails to respond, i.e., to expand, accordingly, and these defects disfavor charge transfer involved in the electrochemical reactions. Every irreversible lattice-expansion and -contraction cycle introduces additional lattice defects, causing gradual capacity fading. In essence, it is suggested that the fading is caused by "nontransition" under excess Li-ion ($x > 1.0$) conditions. The huge increase in charge-transfer resistance at $x > 1.0$, as detected by the impedance analysis (Fig. 7b), is likely due to the presence of such a Li-rich nonequilibrium layer, where insertion of additional Li ions became very difficult.

The in situ synchrotron XRD data indicated that the oxide coating leads to less lattice contraction upon delithiation (charge). It is not difficult to comprehend that reduced lattice contraction would facilitate Li insertion during the next lithiation (discharge) step, and hence improve cycling stability. Indeed, a more open lattice structure could facilitate the reaction kinetic, which in turn leads to an observed reduction in reaction impedance. It is, however, more out of expectation that the Zr oxide coating causes such a modification in lattice variation. Cho et al.,[18,19] in their studying the effect of oxide coatings on cycling performance of $LiCoO_2$, observed reduced lattice expansion upon delithiation (charge) at the same C rate (0.5 C), and they attributed it to the presence of a fracture-toughened surface oxide layer which restrains the electrode material to undergo expansion. This work represents the first observation of reduced lattice contraction by surface coating. One possible cause is that the rigidity of the oxide coating, in combination with the strong bonding between the layer and the spinel particle, helps to accommodate the lattice stress resulting from extraction of Li ions during charge. We believe more definite mechanism(s) for the coating-effected modification of lattice contraction/expansion will require detailed microscopy study.

As a final note, Thackeray et al.[15] once showed that the high-temperature cycling stability of the spinel is significantly improved by surface coating of amorphous Zr oxide, and it was attributed to the reduced solubility of the spinel as a result of scavenge of acidic HF by the Zr oxide layer. To evaluate the significance of the acid-scavenge effect in the present study, amorphous Zr oxide powder was prepared under the same conditions as in the coating process, and electrodes were made from mixture powder consisting of spinel and the Zr oxide powder in a 95:5 weight ratio. It was found that the capacity of this mixture-powder electrode faded as fast as the 0% electrode. This result may suggest that the acid-scavenge effect, if any, is not sufficient to account for improved high-rate stability observed in the current study, which was carried out mainly at RT.

National Taiwan University assisted in meeting the publication costs of this article.

References

1. M. M. Thackeray, P. G. David, P. G. Bruce, and J. B. Goodenough, *Mater. Res. Bull.*, **18**, 461 (1983).
2. D. Guyomard and J. M. Tarascon, *J. Electrochem. Soc.*, **139**, 937 (1992).
3. S. H. Park, K. S. Park, Y. K. Sun, and K. S. Nahm, *J. Electrochem. Soc.*, **147**, 2116 (2000).
4. D. D. MacNeil, T. D. Hatchard, and J. R. Dahn, *J. Electrochem. Soc.*, **148**, A663

(2001).
5. Z. H. Lu, Z. H. Chen, J. R. Dahn, and D. D. MacNeil, *J. Power Sources*, **108**, 8 (2002).
6. H. Haung, C. H. Chen, R. C. Perego, E. M. Kelder, L. Chen, J. Schoonman, W. J. Weydanz, and D. W. Nielsen, *Solid State Ionics*, **127**, 31 (2000).
7. X. Sun, X. Q. Yang, M. Balasubramanian, J. McBreen, Y. Xia, and T. Sakai, *J. Electrochem. Soc.*, **149**, 842 (2002).
8. A. Yamada, M. Tanaka, K. Tanaka, and K. Sekai, *J. Power Sources*, **81**, 73 (1999).
9. G. G. Amatucci, C. N. Schmutz, A. Blyr, C. Sigala, A. S. Gozdz, D. Larcher, and J. M. Tarascon, *J. Power Sources*, **69**, 11 (1997).
10. M. M. Thacheray, S. H. Yang, A. J. Kahaian, K. D. Kepler, E. Skinner, J. T. Vaughey, and S. A. Hackney, *Electrochem. Solid-State Lett.*, **1**, 7 (1998).
11. R. J. Gummow, A. de Kock, and M. M. Thacheray, *Solid State Ionics*, **69**, 59 (1994).
12. G. Amatucci, A. Du Pasquier, A. Blyr, T. Zheng, and J. M. Tarascon, *Electrochim. Acta*, **45**, 255 (1999).
13. M. M. Thacheray, *Prog. Solid State Chem.*, **25**, 1 (1997).
14. J. M. Tarascon, U.S. Pat. 6,295,714 (2003).
15. M. M. Thackeray, C. S. Johnson, J. S. Kim, K. C. Lauzze, J. T. Vaughey, N. Dietz, D. Abraham, S. A. Hackney, W. Zeltner, and M. A. Anderson, *Electrochem. Commun.*, **5**, 752 (2003).
16. A. Hammersley, *FIT2D V10.3 Reference Manual V4.0*, ESRF, Grenoble, France (1998).
17. S. Dash, D. D. Sood, and R. Prasad, *J. Nucl. Mater.*, **228**, 83 (1996).
18. J. Cho, Y. J. Kim, T. J. Kim, and B. Park, *Angew. Chem., Int. Ed.*, **40**, 3367 (2001).
19. J. Cho, Y. J. Kim, and B. Park, *J. Electrochem. Soc.*, **148**, 1110 (2001).